Received: 3 March 2018 | Revised: 1 July 2018 | Accepted: 1 August 2018

DOI: 10.4218/etrij.2018-0116

ORIGINAL ARTICLE

WILEY ETRI Journal

Performance analysis of WPM-based transmission with equalization-aware bit loading

Sarbagya Buddhacharya | **Poompat Saengudomlert**

Bangkok University-Center of Research in Optoelectronics, Communications, and Computational Systems, Bangkok University, Pathum Thani, Thailand.

Correspondence
Sarbagya Buddhacharya, Bangkok University-Center of Research in Optoelectronics, Communications, and Computational Systems, Bangkok University, Pathum Thani, Thailand.
Email: sarbagya.buddhacharya@gmail.com

Funding information
Bangkok University Teaching Assistance Scholarship.

Wavelet packet modulation (WPM) is a multicarrier modulation (MCM) technique that has emerged as a potential alternative to the widely used orthogonal frequency-division multiplexing (OFDM) method. Because WPM has overlapped symbols, equalization cannot rely on the use of the cyclic prefix (CP), which is used in OFDM. This study applies linear minimum mean-square error (MMSE) equalization in the time domain instead of in the frequency domain to achieve low computational complexity. With a modest equalizer filter length, the imperfection of MMSE equalization results in subcarrier attenuation and noise amplification, which are considered in the development of a bit-loading algorithm. Analytical expressions for the bit error rate (BER) performance are derived and validated using simulation results. A performance evaluation is carried out in different test scenarios as per Recommendation ITU-R M.1225. Numerical results show that WPM with equalization-aware bit loading outperforms OFDM with bit loading. Because previous comparisons between WPM and OFDM did not include bit loading, the results obtained provide additional evidence of the benefits of WPM over OFDM.

KEYWORDS
bit loading, minimum mean-square error equalization, multicarrier modulation, wavelet packet modulation

1 | INTRODUCTION

Multicarrier modulation (MCM) has been extensively used to support the ever-growing demands of large data rates using limited bandwidth. While orthogonal frequency-division multiplexing (OFDM) is a widely adopted MCM technique, it has some limitations, such as high signal peak-to-average power ratios (PAPRs), high spectral sidelobes due to the use of rectangular time windows, and the need for complex multiplications, even for applications using real signals. Owing to these limitations, several alternatives to OFDM have been proposed, among which wavelet packet modulation (WPM) is considered as an attractive candidate [1–5]. OFDM is based on the Fourier transform, and uses the inverse fast Fourier transform (IFFT) at the transmitter and the fast Fourier transform (FFT) at the receiver. Meanwhile, WPM is based on a multirate filter tree structure that computes the inverse discrete wavelet packet transform (IDWPT) at the transmitter and the discrete WPT (DWPT) at the receiver. In OFDM, the symbols to be transmitted on subcarriers are generated by the IFFT, which has a fixed computational structure. Unlike OFDM, WPM uses IDWPT, which has a flexible filter tree structure that can easily be modified by changing the filter coefficients [6]. In addition, the iterative tree structure allows the simple reconfiguration of the transform size according to the channel characteristics [7].

The PAPR for WPM has been investigated in [6,8,9]. In [6], statistics of WPM signals and their power distributions are analyzed along with the impact on the PAPR owing to

different wavelet families and wavelet filter lengths. The results show that orthogonal wavelets from different wavelet families have similar PAPR distributions that are also independent of the wavelet filter length. This work is further extended to reduce the PAPR by generating a set of WPM frames with random phase shifts on subcarriers, and by selecting a set that has the lowest PAPR [8]. In [9], it is shown that WPM reduces the PAPR significantly when compared to OFDM for a small number of subcarriers, while for a large number of subcarriers, both modulations have similar PAPR performances.

With MCM, we can perform equalization and bit loading to improve transmission performances. In OFDM, equalization can be achieved using cyclic prefixes (CPs) and one-tap equalization. However, the use of the CP is not practical for WPM as the output length of IDWPT is longer than the input length (number of subcarriers), resulting in overlaps between successive WPM symbols in the time domain. Equalization for WPM can be performed in the time domain before passing the equalized signal through DWPT to recover data symbols on subcarriers in the frequency domain. Instead of such a time-domain equalization, equalization can also be done after DWPT in the frequency domain. The time-domain equalization for WPM is explored in [10–14], while the frequency-domain equalization is studied in [7,14].

In [10], a nonideal channel is considered with multiple subcarriers, each of which is characterized by attenuation and delay. These subbands are represented by narrowband orthonormal wavelets, which encounter delay and attenuation. Equalization is thus reduced to estimating the delay and attenuation for each subcarrier. An algorithm called the minimum square variance (MSV) is applied to reduce the intersymbol interference (ISI) using the variance of the demodulated output. This approach suffers from high computational complexity when the number of subcarriers increases. The use of time-domain equalization for WPM using the peak distortion criterion to reduce the maximum ISI is proposed in [11], which also explores the impact of different wavelet families, wavelet filter lengths, and the number of equalizer taps on the equalization performance. This method is limited to the removal of ISI, and does not include the removal of intercarrier interference (ICI). In [12,13], a frequency-domain zero-forcing (ZF) equalizer and a time-domain MMSE equalizer are proposed for WPM. The results show that WPM with time-domain MMSE equalization is better than WPM with frequency-domain ZF equalization, and it is also better than OFDM employing a CP with one-tap equalization. In [7], frequency-domain equalization for WPM is introduced, but requires a combined time-frequency equalization structure that is much more complex than time-domain equalization. In [14], frequency-domain equalization is performed using the channel estimates based on least-square (LS) and linear MMSE criteria. Training sequences are transmitted as pilot signals for channel estimation. The results showed that equalization using channel estimates from linear MMSE performs better than that obtained with the LS method.

Bit loading is a technique that allocates fewer bits to subcarriers that are more affected by channel distortions, resulting in an enhanced bit error rate (BER) performance. Bit loading for OFDM has been widely studied, but few studies have explored bit loading for WPM [15,16]. In [15], bit loading is done adaptively based on the channel variation across subcarriers to achieve the minimum total transmit power according to the desirable quality of service (QOS) and BER. However, the proposed bit loading does not consider equalization or any other signal processing to overcome ISI caused by channel dispersion. In [16], bit loading is performed along with a unitary mapping filter that is used to remove ICI. In order to eliminate ISI, guard chips are inserted between successive WPM symbols. The technique is equivalent to zero padding at the end of each WPM symbol, and becomes inefficient when WPM symbols are long owing to the large overhead from zero padding.

Recent studies for WPM include PAPR reduction [17–19], as well as spectrum sensing (SS) for cognitive radio (CR) [20]. PAPR reduction for WPM using adaptive wavelet packet modulation (AWPM) is proposed in [17], and relies on the trade-off between PAPR and BER. The proposed algorithm identifies the frequency range over which the channel is frequency selective, and performs bandwidth division to help reduce the BER. A PAPR reduction method for WPM with partial transmit sequences (PTSs) and a tree-pruning approach are presented in [18]. In [19], the PTS approach is considered with embedded side information (ESI) in the transmit frame. In [20], the SS approaches for CR are proposed based on the accumulated time-domain symbol cross-correlation (ATDSC) and accumulated wavelet-domain symbol cross-correlation (AWDSC). Because these approaches require a significant number of pilot signals, another method that is based on approximated covariance matrices is proposed to reduce the requirements.

To the best of the authors' knowledge, studies that have been performed to date have not reported a concrete procedure for the bit-loading algorithm in the case of WPM with equalization. The main contribution of this paper is to present a bit-loading algorithm for WPM that incorporates noise amplification and signal attenuation owing to the imperfection of MMSE equalization. In addition, a mathematical expression for the BER performance is derived and verified using simulation results. The derived BER expression is used to quantify the advantage of bit loading and for comparison with OFDM. The rest of the paper is organized as follows. The system model is given in Section 2, and the bit-loading algorithm is presented in Section 3. A mathematical analysis of the BER

performance is given in Section 4, after which simulation results are presented in Section 5. The system performance analysis is presented in Section 6. Finally, the paper is concluded in Section 7.

2 | SYSTEM MODEL

Figure 1A shows the overall block diagram for a WPM system with bit loading and time-domain equalization. Bit allocation to each subcarrier is done using a bit-loading algorithm, in the absence of which all of the subcarriers will have the same number of bits per symbol. Bit loading is followed by a serial-to-parallel converter whose output is fed to quadrature amplitude modulation (QAM) mapping in order to generate QAM symbols. The IDWPT unit takes QAM symbols as inputs, and generates time-domain WPM symbols that are transmitted through the channel. The transmitted signal is convolved with the channel impulse response (CIR), and is then added to the additive white Gaussian noise (AWGN). The received signal is first passed through a time-domain MMSE equalizer to undo the channel distortion, and then to the DWPT to obtain the received QAM symbols. After QAM demapping and a parallel-to-serial converter, received data bits are obtained. The difference between the transmitted data bits and received data bits will give the BER.

In Figure 1A, IDWPT is employed to generate the transmit complex data sequence s_n from QAM symbols S_k,

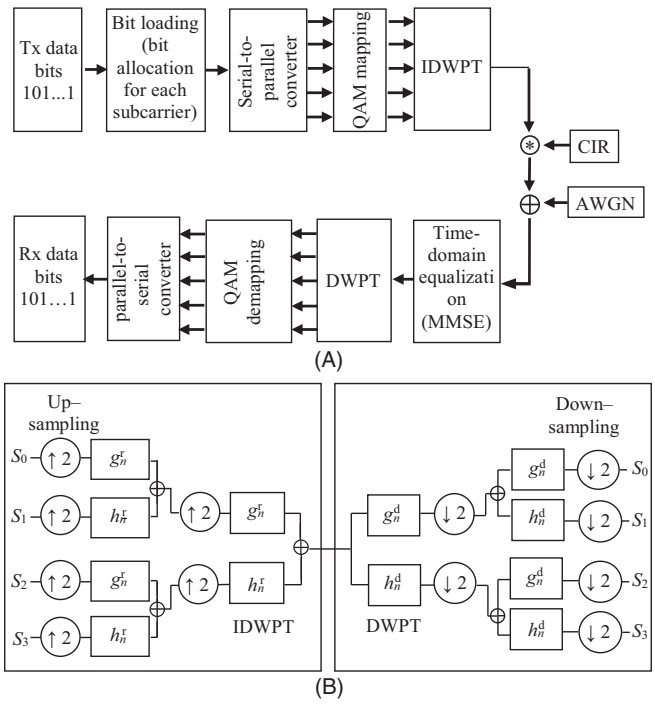

FIGURE 1 (A) WPM system block diagram, (B) IDWPT and DWPT with two stages

where n is the time index and k is the subcarrier index. The signal for each WPM symbol is given by an orthonormal expansion [21]:

$$s_n = \sum_{k=0}^{N-1} S_k \phi_n^k, \tag{1}$$

where ϕ_n^k is the basis function of subcarrier k, which is the IDWPT output in Figure 1B when the only nonzero input is $S_k = 1$. Denote the CIR of length C by h_n. Let w_n be a complex AWGN sequence with mean zero and variance N_0. The received signal r_n can be written as:

$$r_n = s_n * h_n + w_n, \tag{2}$$

where the notation * represents the convolution operation. The received signal r_n is passed through a time-domain linear MMSE equalizer having equalizer coefficients f_n, yielding the output signal:

$$y_n = r_n * f_n. \tag{3}$$

Then, y_n is passed through the DWPT unit to recover QAM symbols.

2.1 | Wavelet packet modulation

The basic building blocks of WPM are low-pass filters (LPFs) and high-pass filters (HPFs), which form quadrature mirror filter (QMF) pairs. The outputs of both LPFs and HPFs are symmetrically decomposed, resulting in an equal bandwidth distribution over the frequency range. The decomposition process is known as the analysis process. The inverse operation, which is a reconstruction process, is known as the synthesis process. Let g_n^{d} and h_n^{d} be the analysis (or decomposition) LPF and HPF, respectively. Similarly, let g_n^{r} and h_n^{r} be the synthesis (or reconstruction) LPF and HPF, respectively. Let F be the filter length. These filter pairs are related to each other by [21]:

$$h_n^{\mathrm{d}} = (-1)^n g_{F-1-n}^{\mathrm{d}}, \tag{4}$$

$$h_n^{\mathrm{r}} = h_{F-1-n}^{\mathrm{d}}, \quad g_n^{\mathrm{r}} = g_{F-1-n}^{\mathrm{d}}. \tag{5}$$

The inverse transform IDWPT is used at the transmitter, while the forward transform DWPT is used at the receiver. The number of inputs for IDWPT is the same as the number of subcarriers, which depends on the number of reconstruction stages. IDWPT is illustrated in Figure 1B, where the number of reconstruction stages is 2, yielding four subcarriers. At each stage, an input signal is passed through upsampling, which is followed by LPF or HPF, after which each output pair is combined. The reverse operation is carried out in DWPT, where an input signal is first passed through LPF and HPF, whose outputs are followed by downsampling. The length of the WPM symbol generated

by IDWPT is generally larger than the number of subcarriers, resulting in overlapping WPM symbols in the time domain. With filter length F and N subcarriers, the length of a WPM symbol is [21]

$$L = (N-1)(F-1)+1. \tag{6}$$

2.2 | Linear MMSE equalization

Equalization was performed to eliminate or reduce the impact of interference and distortion introduced by the channel. We used a linear MMSE equalizer that operates in the time domain [22]. When the CIR is unknown, a known training sequence is used, with equalizer coefficients chosen such that the mean-square error (MSE) between the equalizer output and the known signal is minimized. The equalizer filter is given by [22]:

$$\mathbf{f} = \left(\mathbf{R}^{\mathrm{T}}\mathbf{R}\right)^{-1}\mathbf{R}^{\mathrm{T}}\mathbf{s}. \tag{7}$$

In (7), $\mathbf{s}$ is a column vector that contains a delayed transmitted training sequence of symbols, and $\mathbf{R}$ is a Toeplitz matrix containing the received signals before equalization. The column vector $\mathbf{f}$ contains E equalizer coefficients, which form a tapped delay line finite-impulse response (FIR) filter.

However, if the CIR is known, equalizer filter coefficients can be derived based on [23], as given by (8). This eliminates the need for a training sequence.

$$\mathbf{f} = \mathbf{\Gamma}^{-1}\xi. \tag{8}$$

In (8), $\mathbf{f}$ is the column vector containing $E = 2K+1$ coefficients of the equalizer. Here, for convenience, E is expressed in terms of K, where K indicates the number of signal values around the symbol of interest. $\mathbf{\Gamma}$ is a $(2K+1)\times(2K+1)$ matrix with element $g_{l,m}$, as given by (9), where $-K \le l$, $m \le K$, l is the row index of $\mathbf{\Gamma}$, and m is the column index of $\mathbf{\Gamma}$. ξ is a column vector containing the CIR, as given by (10). In ξ, the first $K-(C-1)$ elements and the last K elements are equal to zero.

$$g_{l,m} \triangleq \textstyle\sum_{k=0}^{C-1} h_{k+m-l}h_k^* + N_0\delta_{m-l}, \tag{9}$$

$$\begin{aligned}\xi &\triangleq \left[\, h_K^* \quad h_{K-1}^* \quad \cdots \quad h_{-K}^* \,\right]^{\mathrm{T}} \\ &= \left[\, 0 \quad \cdots \quad 0 \quad h_{C-1}^* \quad \cdots \quad h_0^* \quad 0 \quad \cdots \quad 0 \,\right]^{\mathrm{T}}.\end{aligned} \tag{10}$$

In (9), the superscript * indicates the complex conjugate operation, and δ represents the impulse function. The equalization MSE can be evaluated using [23] as:

$$\mathrm{MSE} \triangleq 1 - \xi^{\dagger}\mathbf{\Gamma}^{-1}\xi, \tag{11}$$

where the notation † represents the conjugate transpose.

3 | EQUALIZATION-AWARE BIT-LOADING ALGORITHM

This section proposes a bit-loading algorithm that considers the equalization error, and which is based on the conventional water-filling technique [24]. However, it also accounts for noise amplification and signal attenuation owing to equalization error. This equalization-aware feature allows the use of a low-complexity equalizer, while maintaining good BER performances.

3.1 | Noise power gain

The noise power gain on each subcarrier can be numerically evaluated by generating AWGN and passing it through the equalizer filter, as shown in Figure 2A. The signal value is set equal to zero so that the output of DWPT is due to noise only. Therefore, the variance of each output signal will give the noise power gain on each subcarrier. Note that this AWGN generation process is only used for the simulation to validate the analytical expression in the following paragraphs. This process is not required in the actual receiver.

The noise power gain on each subcarrier can also be derived analytically using the equivalent signal processing block diagram, as shown in Figure 2B. At the receiver, after the equalizer filter, the QAM symbol on subcarrier k is obtained by passing the WPM symbol through the matched filter ϕ_{-n}^{k}, followed by sampling, which is the standard procedure employed to retrieve the coefficient of an orthonormal expansion in (1) [23]. In addition, W_k denotes the output after sampling on subcarrier k.

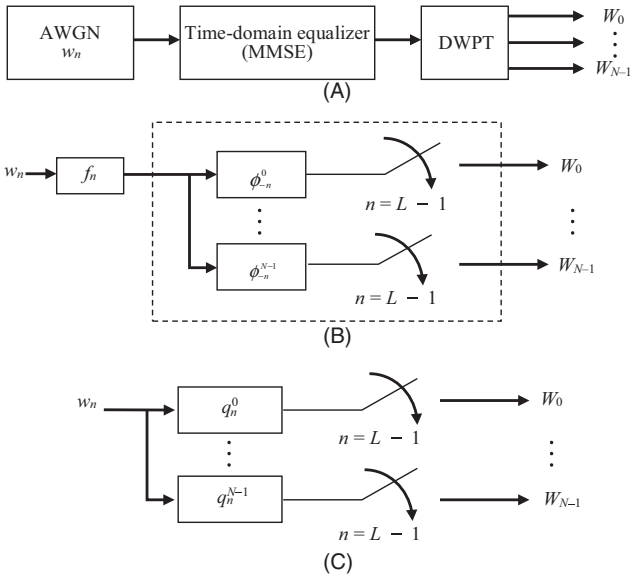

FIGURE 2 Block diagram for computation of noise power gains on subcarriers for WPM (A) using simulations, (B) using analysis, (C) using analysis based on an equivalent filter

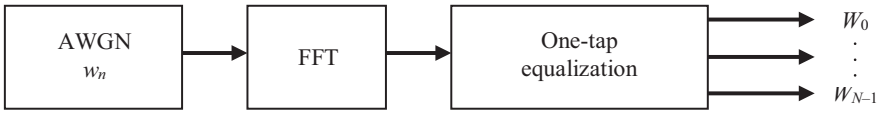

FIGURE 3 Block diagram for computation of noise power gains on subcarriers for OFDM using simulation

The equalizer filter f_n and the matched filter ϕ^k_{-n} can be combined to form an equivalent filter given by (12). The equivalent block diagram is shown in Figure 2C.

$$q^k_n = f_n * \phi^k_{-n}. \tag{12}$$

When any random process is passed through a linear time invariant (LTI) filter, the power spectral density (PSD) of the output will be equal to the PSD of the input multiplied by the squared norm of a vector containing filter coefficients [25]. Therefore, the noise power gain on subcarrier k, which is denoted by γ_k and which is equivalent to the variance of W_k divided by N_0, can be evaluated using:

$$\gamma_k = \mathrm{var}[W_k]/N_0 = ||q^k_n||^2. \tag{13}$$

In the case of OFDM with the CP, the noise power on each subcarrier can be obtained by passing AWGN through the process shown in Figure 3. The variance of each output of one-tap equalization will give the noise power on each subcarrier. The use of the CP enables OFDM to implement one-tap equalization, which is accomplished by multiplying a received data symbol on subcarrier k by the inverse of the subcarrier gain $1/H_k$ where H_k is the FFT of CIR h_n. Therefore, the noise power amplification factor is $1/|H_k|^2$ [24]. In light of this fact, for OFDM, the noise power gain on subcarrier k is:

$$\gamma_k = \mathrm{var}[W_k]/N_0 = 1/|H_k|^2. \tag{14}$$

3.2 | Signal power gain

The signal power gains for WPM can be evaluated using the transmission path, as shown in Figure 4A. The transmit signal is passed through the channel and the MMSE equalizer filter, which is followed by DWPT. Here, noise is assumed equal to zero so that the output is only due to signal values.

An equivalent block diagram that is used to obtain signal power gains analytically is shown in Figure 4B. For subcarrier k, there are channel filter h_n, equalizer filter f_n, and matched filter ϕ^k_{-n}, followed by a sampler. The expression for the signal power gain on subcarrier k, which is denoted by η_k, is given by:

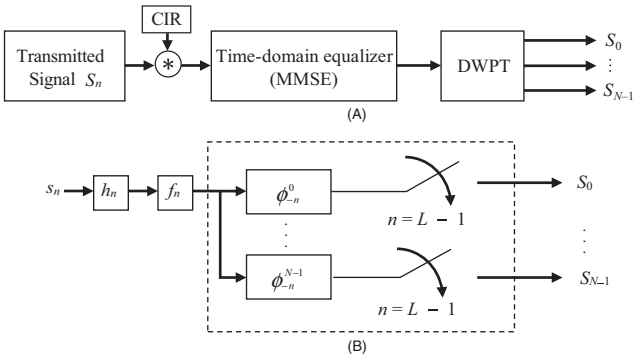

FIGURE 4 Block diagram for computation of signal power gains on subcarriers for WPM (A) using simulations, and (B) using analysis

$$\eta_k = \left|\left\langle f_n * h_n * \phi^k_n, \phi^k_n \right\rangle\right|^2, \tag{15}$$

where $\langle . , . \rangle$ denotes the inner product operation between two signals. For OFDM, one-tap equalization yields a signal power gain value of 1 for all subcarriers.

3.3 | Signal power computation

In the bit-loading algorithm, two bits are added to one subcarrier in each iteration because we consider square QAM constellations. Let E'_b be the received energy per bit. The values of E'_b/N_0 that are required for $M \times M$ QAM to obtain a BER of 10^{-5} are listed in Table 1. These E'_b/N_0 values can be obtained using (16), which is derived based on the union bound estimate for uncoded transmissions [26].

$$\mathrm{BER} \approx \frac{2(M-1)}{M \log_2 M} Q\left(\sqrt{\left(\frac{6 \log_2 M}{M^2 - 1}\right) \times \frac{E'_b}{N_0}}\right). \tag{16}$$

In (16),

$$Q(x) = \frac{1}{\sqrt{2\pi}} \int_x^\infty e^{-(z^2)/2} dz.$$

TABLE 1 E'_b/N_0 for $M \times M$ QAM with BER = 10^{-5}

M	No. of bits per QAM symbol	Required E'_b/N_0 (dB)
2	2	9.6
4	4	13.4
8	6	17.8
16	8	22.5

3.4 | Bit loading

Bit loading on subcarriers is achieved using an iterative algorithm that is based on signal and noise power gains across the subcarriers. In addition to noise amplification and signal attenuation, the equalization error introduces ICI. However, it is not straightforward to consider ICI for bit loading because the ICI induced on each subcarrier depends on the signal powers on all the subcarriers, which in turn depends on the number of bits allocated to all of the subcarriers. In short, the ICI and bit allocation are interrelated. In addition, as will be shown in a later section, the ICI values are negligible when compared to the noise powers. Therefore, the ICI is not considered in the bit-allocation process. The numerical results that are presented in a later section show that WPM still performs better than OFDM, even when ICI is not considered for bit allocation.

The flowchart for the bit-loading algorithm is shown in Figure 5. First, the ratio γ_k/η_k is calculated for each subcarrier k and corresponds to the normalized noise power $(\gamma_k N_0/\eta_k)$, with the constant N_0 omitted (to be explained shortly). It serves as the initial water level denoted by Z_k . At the beginning of each iteration, two bits are added to each subcarrier, and the water level Z_k is updated with respect to the additional two bits using:

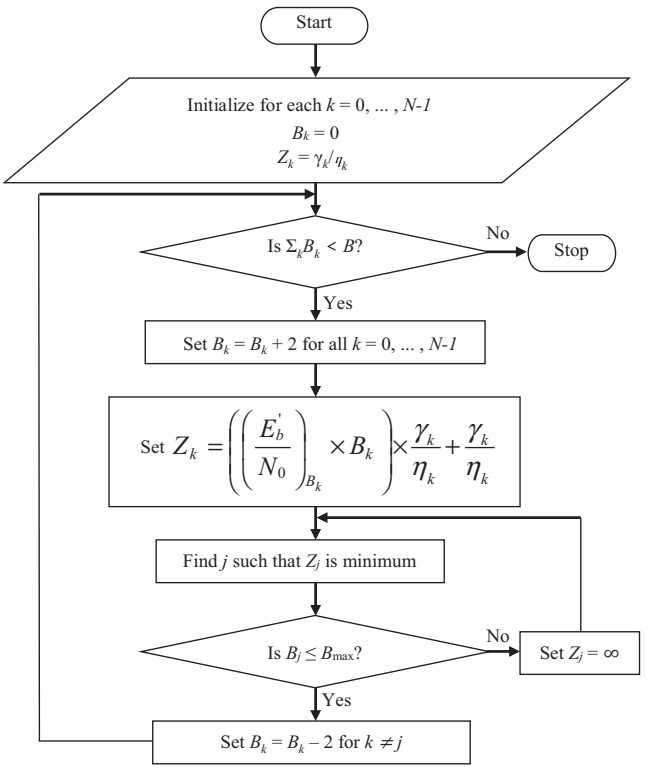

FIGURE 5 Flowchart for bit-loading algorithm

$$Z_k = \left(\left(\frac{E'_b}{N_0}\right)_{B_k} \times B_k\right) \times \frac{\gamma_k}{\eta_k} + \frac{\gamma_k}{\eta_k}, \tag{17}$$

where B_k indicates the number of bits on subcarrier k and $(E'_b/N_0)_{B_k}$ is the value of E'_b/N_0 that is required for subcarrier k to transmit B_k bits per symbol, as listed in Table 1. Because E'_b/N_0 is considered as the SNR per bit [23], the term $(E'_b/N_0)_{B_k} \times B_k$ in (17) corresponds to the SNR, yielding a signal power value that is equal to the first term on the right-hand side of (17), with the constant N_0 omitted. Therefore, Z_k in (17) can be viewed as the sum of signal and noise powers. Because the water level values of Z_k are used for comparison only, it is possible to omit the common multiplicative factor N_0 from both the signal and noise powers. Then, the subcarrier j with the minimum water level and $B_j \le B_{\max}$ is selected. At the end of each iteration, B_k is reduced by 2 for each subcarrier $k \neq j$. This is equivalent to assigning two bits to subcarrier j which minimizes the maximum water level after the assignment. The process is repeated until the total number of allocated bits is equal to the desired number of bits B which is assumed to be twice the number of subcarriers, that is, 2×2 QAM on each subcarrier without bit loading.

The value of $B_{\max}$ is set to 8, resulting in possible constellations being 2×2 QAM, 4×4 QAM, 8×8 QAM, and 16×16 QAM. The process can be extended beyond 16×16 QAM, but numerical results indicate that larger constellations are not needed.

4 | MATHEMATICAL ANALYSIS FOR BER COMPUTATION

4.1 | BER analysis for WPM

The BER expression for WPM can be derived in terms of E_b/N_0, where E_b is the transmit energy per bit. Here, let E_c denote the energy per channel use, let M_k denote the constellation size of $M_k \times M_k$ QAM for subcarrier k, and let N denote the number of subcarriers. Finally, let $d_{\min}$ denote the minimum distance between the signal points, which is assumed to be the same for all of the signal sets. Because the average symbol energy of $M_k \times M_k$ QAM is $d^2_{\min}(M_k^2 - 1)/6$ [26], the energy per channel use can be written as [26]:

$$E_c = \frac{1}{N}\left(\sum_{k=0}^{N-1}\left(\frac{M_k^2 - 1}{6}\right)\right) d^2_{\min}. \tag{18}$$

For each WPM symbol period, the energy per WPM symbol can be written as the product of the number of channel uses (i.e., the number of transmitted values) and the energy per channel use, or equivalently, the product of the number of information bits transmitted and the energy

per information bit. It follows that:

$$N \times E_c = \left(\sum_{k=0}^{N-1} 2\log_2 M_k\right) \times E_b, \tag{19}$$

yielding

$$E_b = \left(\frac{N}{\sum_{k=0}^{N-1} 2\log_2 M_k}\right) \times E_c. \tag{20}$$

The constellation size M_k for subcarrier k depends on the bit allocation obtained from the bit-loading algorithm. By substituting E_c from (18), $d_{\min}$ can be obtained as:

$$d_{\min} = \sqrt{\frac{\sum_{k=0}^{N-1} 2\log_2 M_k}{\sum_{l=0}^{N-1}\left(\frac{M_l^2-1}{6}\right)} \times E_b}. \tag{21}$$

At the receiver, E_b is scaled by the signal power gain η_k on subcarrier k. The expression for $d_{\min}$ at the receiver becomes

$$d'_{\min} = \sqrt{\frac{\sum_{k=0}^{N-1} 2\log_2 M_k}{\sum_{l=0}^{N-1}\left(\frac{M_l^2-1}{6}\right)} \times \eta_k E_b}. \tag{22}$$

The BER for subcarrier k considering $M_k \times M_k$ QAM can be obtained using the union bound estimate [26]:

$$\mathrm{BER}_k \approx \frac{2(M_k-1)}{M_k \log_2 M_k} Q\left(\frac{d'_{\min}}{\sqrt{2N_k^{\mathrm{I}}}}\right), \tag{23}$$

where N_k^{I} is the equivalent interference-plus-noise power on subcarrier k, which includes noise power as well as ICI. The ICI on subcarrier k from subcarrier j can be calculated as:

$$\beta_{k,j} = \left|\left\langle h_n * f_n * \phi_n^j,\ \phi_n^k \right\rangle\right|^2. \tag{24}$$

Accordingly, the total ICI on subcarrier k from all other subcarriers j such that $j \neq k$ is given by:

$$\beta_k^{\mathrm{total}} = \sum_{j=0, j\neq k}^{N-1} \beta_{k,j}. \tag{25}$$

Hence, N_k^I can be expressed as:

$$N_k^{\mathrm{I}} = \gamma_k N_0 + \beta_k^{\mathrm{total}}. \tag{26}$$

Substituting $d'_{\min}$ from (22) and N_k^{I} from (26) in (23), BER_k can be expressed as:

$$\mathrm{BER}_k \approx \frac{2(M_k-1)}{M_k \log_2 M_k} \times Q\left(\sqrt{\left(\frac{\sum_{i=0}^{N-1} 2\log_2 M_i}{\sum_{l=0}^{N-1}\left(\frac{M_l^2-1}{6}\right)}\right) \times \frac{1}{2} \times \frac{\eta_k E_b}{\gamma_k N_0 + \beta_k^{\mathrm{total}}}}\right). \tag{27}$$

The overall BER can be calculated using the weighted average of the BERs on all subcarriers, as given by:

$$\mathrm{BER} \approx \sum_{k=0}^{N-1} \frac{2\log_2 M_k}{\sum_{l=0}^{N-1} 2\log_2 M_l} \times \mathrm{BER}_k. \tag{28}$$

4.2 | BER analysis for OFDM

The BER expression can be derived for OFDM with the CP in a similar fashion. The CP length is denoted by N_c. For OFDM, the energy per OFDM symbol can be written as:

$$(N + N_c) \times E_c = \left(\sum_{k=0}^{N-1} 2\log_2 M_k\right) \times E_b. \tag{29}$$

yielding

$$E_b = \left(\frac{N + N_c}{\sum_{k=0}^{N-1} 2\log_2 M_k}\right) \times E_c. \tag{30}$$

Substituting E_c from (18), the expression for $d_{\min}$ can be obtained as:

$$d_{\min} = \sqrt{\frac{N}{N+N_c}\left(\frac{\sum_{k=0}^{N-1} 2\log_2 M_k}{\sum_{l=0}^{N-1}\left(\frac{M_l-1}{6}\right)}\right) \times E_b}. \tag{31}$$

Using (23), the BER expression for subcarrier k can be derived with N_k^{I} equal to $N_0/|H_k|^2$, with H_k being the FFT of the CIR.

$$\mathrm{BER}_k \approx \frac{2(M_k-1)}{M_k \log_2 M_k} \times Q\left(\sqrt{\frac{N}{N+N_c}\left(\frac{\sum_{i=0}^{N-1} 2\log_2 M_i}{\sum_{l=0}^{N-1}\left(\frac{M_l^2-1}{6}\right)}\right) \times \frac{|H_k|^2}{2} \times \frac{E_b}{N_0}}\right). \tag{32}$$

The overall BER can be calculated using (28), as in the case for WPM.

The BER on each subcarrier for WPM is given by (27), while the BER on each subcarrier for OFDM is given by (32). The overall BER is given by (28). These analytical expressions are validated by performing simulations, and the results are shown in Section 5. After the validation, they are used to compare the performances of WPM and OFDM in Section 6.

4.3 | Computational complexity

The computation complexity of N-point IDWPT/DWPT is of the order of $O(N\log_2 N)$ [21], which is similar to the complexity of IFFT/FFT. In addition, for linear MMSE equalization, the number of operations required per signal value is of the order of the equalizer filter length, that is,

constant E, yielding a complexity of the order of $O(N)$ per WPM symbol. Therefore, the overall computational complexity of WPM is of the order of $O(N \log_2 N)$, which is the same as for OFDM.

5 | SIMULATION RESULTS

The analytical BER expressions derived in previous sections were verified using numerical results obtained from a simulation program that was written using MATLAB according to the block diagram in Figure 1A. The simulations were carried out for three different test environments as per Rec. ITU-R M.1225 [27]. The three test environments are: (i) indoor office test environment, (ii) outdoor to indoor and pedestrian test environment, and (iii) vehicular test environment. Each test environment has two channels, that is, channel A and channel B. The other simulation parameters are listed in Table 2.

The MMSE equalizer coefficients that were obtained using the analytical expression in (8) were compared with the equalizer coefficients obtained by (7) using a randomly generated but known training sequence of 10 WPM symbols. Channel A was used for the indoor office test environment, and the equalizer filter with 41 taps was obtained. The results in Figure 6A-B show that the equalizer filter coefficients generated by the expression in (8) are close to the equalizer filter coefficients that were obtained using (7) with a known training sequence. Hence, the filter coefficients in (8) can also be used to evaluate the transmission performances under quasistatic channels when training is done occasionally to adapt to channel changes, for example, owing to slow fading. In addition, for further investigation, the equalizer filter coefficients in (8) were used. Figure 6C shows the histogram plot of equalization errors from QAM symbols obtained from simulation results of 500 transmitted WPM symbols. The plot shows that the equalization error has a Gaussian distribution. Unlike in the case of single-carrier modulation where the equalization error is generally not Gaussian [23], the equalization error in our case is passed through DWPT at the receiver, resulting in a Gaussian distribution. This equalization error could not be added directly to the noise variance, but it is incorporated as noise power amplification, signal power attenuation, and ICI.

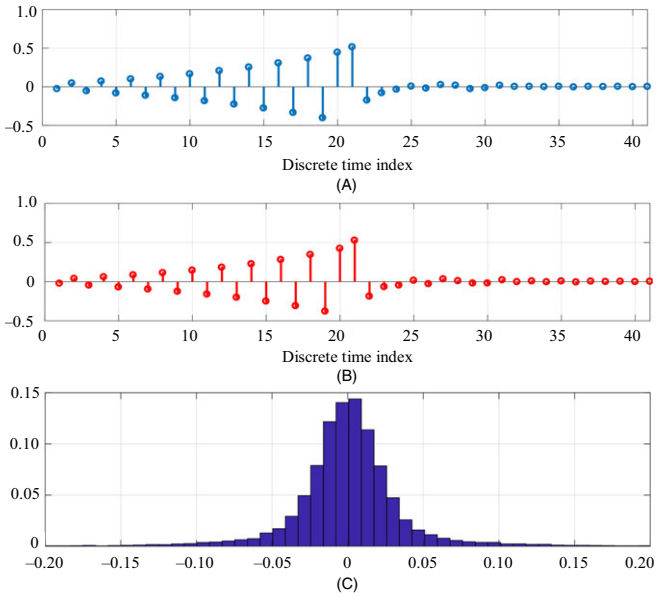

FIGURE 6 Equalizer filter coefficients for channel A of indoor office test environment (A) using training sequence, (B) using the expression in (8), (C) distribution of equalization error for equalizer coefficient in (B)

TABLE 2 Simulation parameters for WPM and OFDM transmissions

Parameter	Value
MCM technique	WPM, OFDM
No. of subcarriers	64
No. of MCM symbols	500
QAM signal sets	2 × 2, 4 × 4, 8 × 8
Wavelet function	db4 [18]

Noise power gains on WPM subcarriers are calculated using (13). Considering channel A for the indoor office environment, the values obtained from (13) are compared with those from the simulation based on Figure 2A. From Figure 7, it can be seen that the noise power gains obtained from the analytical expression are close to the simulation results. Hence, for further performance analysis, the analytical expression is considered.

Based on the noise power gain distribution obtained from Figure 7, it can be observed that noise power gains are not sorted in increasing order. This is because in

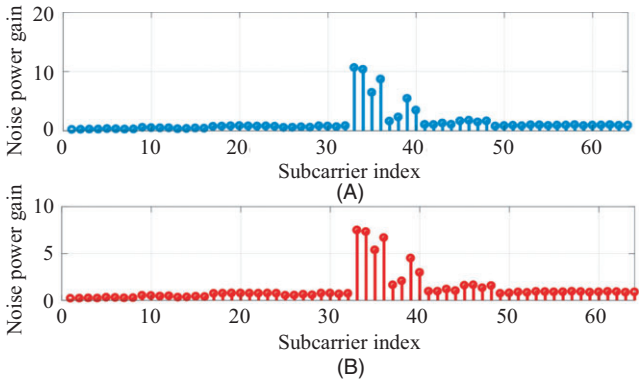

FIGURE 7 Noise power gains across all subcarriers for channel A of indoor office test environment (A) using simulation, (B) using the expression in (13)

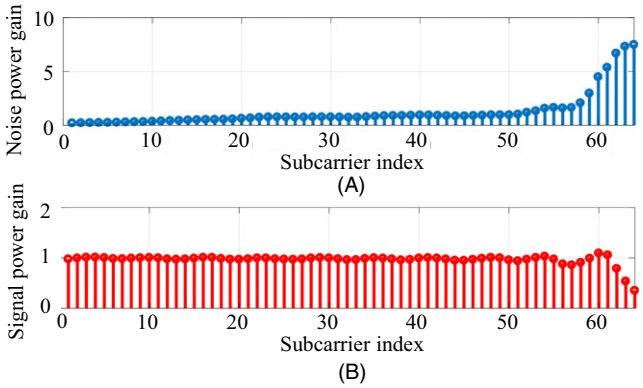

FIGURE 8 (A) Noise power gains, (B) signal power gains across all subcarriers rearranged from low- to high-frequency components for channel A of indoor office test environment

DWPT, as shown in Figure 1B, the outputs of each LPF-and-HPF pair are further passed through LPF and HPF, followed by a downsampling of rate 2. The frequency order at the LPF output after decimation remains intact. However, at the HPF output after decimation, high- and low-frequency components are swapped, which is also known as band-shuffling [28]. As WPM has a symmetric tree structure and this swapping of frequency components occurs only at the HPF outputs, the frequency components are reordered according to the gray code sequence [1,28]. The noise power gains across subcarriers rearranged from low- to high-frequency components are shown in Figure 8A. Similarly, the signal power gains across subcarriers obtained using (15) and rearranged from low- to high-frequency components are shown in Figure 8B. In the plot, signal power gains for subcarriers at high frequencies are less than unity, demonstrating that for high frequencies, equalization is not perfect. However, the impact on the BER owing to this imperfection is overcome by the proposed bit-loading algorithm.

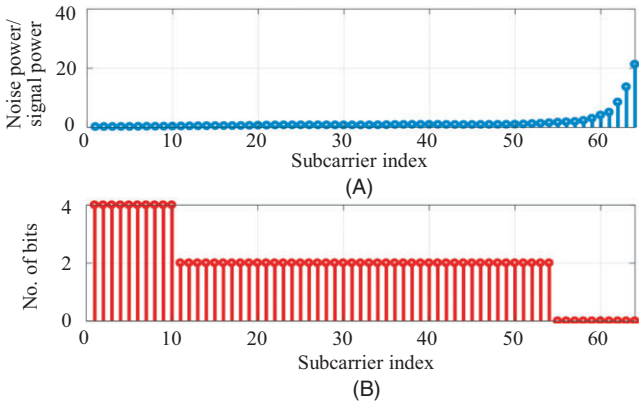

FIGURE 9 (A) Noise power gain to signal power gain across all subcarriers rearranged from low- to high-frequency components for channel A of indoor office test environment (B) bit allocation on all subcarriers for channel A of indoor office test environment

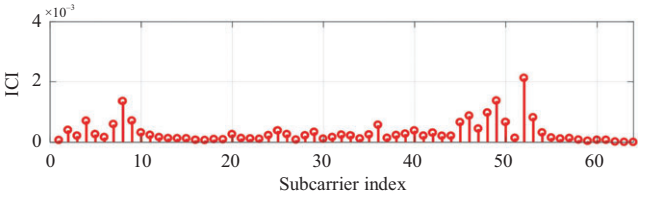

FIGURE 10 ICI across all subcarriers with bit allocation for channel A of indoor office test environment as shown in Figure 9B

Next, bit allocation is performed using the proposed bit-loading algorithm in Section 3. The plot for the ratios of noise and signal power gains is shown in Figure 9A, with the corresponding bit allocation shown in Figure 9B. From the figure, it can be seen that more bits are allocated to subcarriers with lower initial water levels. Assuming $N_0 = 1$ without loss of generality, the ICI for each subcarrier is computed using (25) according to the bit allocation in Figure 9B. The ICI values are within the range of 10^{-3}, as shown in Figure 10. These ICI values are quite low compared to noise powers (equal to noise power gains because $N_0 = 1$), as shown in Figure 8A. Therefore, it is reasonable to ignore ICI values in the bit-loading algorithm as the contribution from ICI is insignificant compared to noise powers.

The BER plots are obtained from the BER expressions derived in Section 4, and are compared with simulation results. For the case of equalization without bit loading, the same QAM constellation is used in all subcarriers, and is chosen to be 2×2 QAM. When equalization with bit loading is considered, the constellation sizes depend on the bit allocation obtained from the bit-loading algorithm. However, we maintain the same number of transmitted bits per WPM symbol for both cases without and with bit loading.

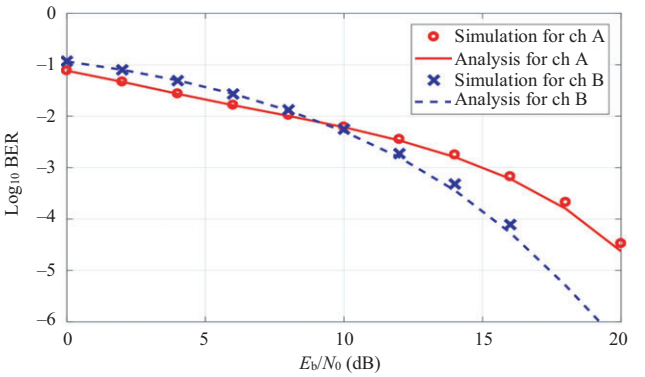

FIGURE 11 BER vs E_b/N_0 for channel A and channel B of indoor office test environment for WPM considering MMSE equalization without bit loading

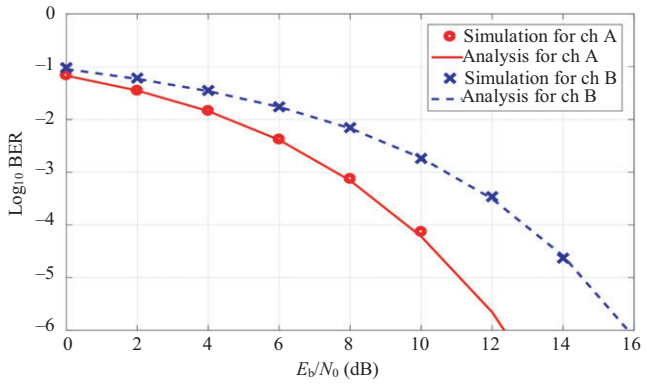

FIGURE 12 BER vs E_b/N_0 for channel A and channel B of indoor office test environment for WPM considering MMSE equalization with bit loading

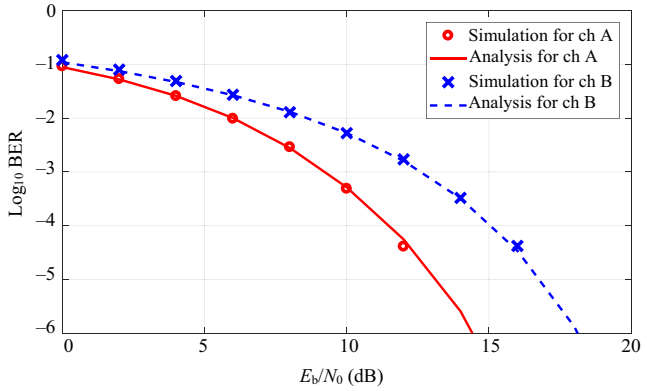

FIGURE 13 BER vs E_b/N_0 for channel A and channel B of indoor office test environment for OFDM considering one-tap equalization with bit loading

The BER plots for WPM with equalization, but without bit loading, are shown in Figure 11. BER plots are drawn using analytical expressions in (27) and (28), and are compared with simulation results for channel A and channel B of the indoor office test environment. Numerical results show that analytical BER values are close to simulation results. Similarly, BER plots for WPM considering equalization with bit loading for channel A and channel B for the indoor office test environment are drawn using analytical expressions, and are compared with simulation results, as shown in Figure 12. The BER plots show that analytical expressions can yield BER plots that are close to those obtained from the simulation.

Furthermore, BERs are plotted for OFDM in order to compare the analytical results from (32) and (28) with simulation results. The BER plots obtained for OFDM with one-tap equalization and with bit loading for channel A and channel B for the indoor office test environment are shown in Figure 13. The BER plots show that the results obtained from analytical expressions agree with the simulation results. Because the BER plots shown in

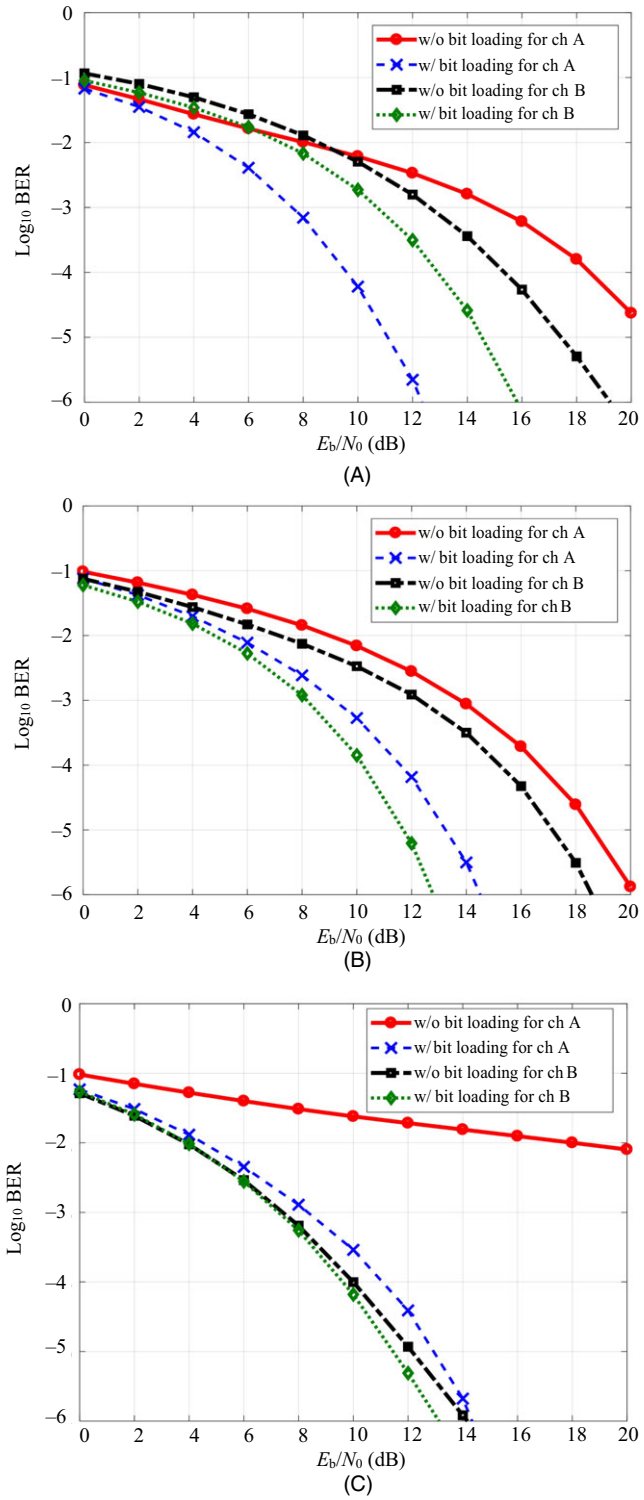

FIGURE 14 BER vs E_b/N_0 using MMSE equalization with and without bit loading for channel A and channel B of (A) indoor office test environment, (B) outdoor to indoor pedestrian test environment, and (C) vehicular test environment

Figures 11–13 show that analytical BER expressions for WPM and OFDM comply with the simulation results, further performance evaluations are based on these analytical BER expressions.

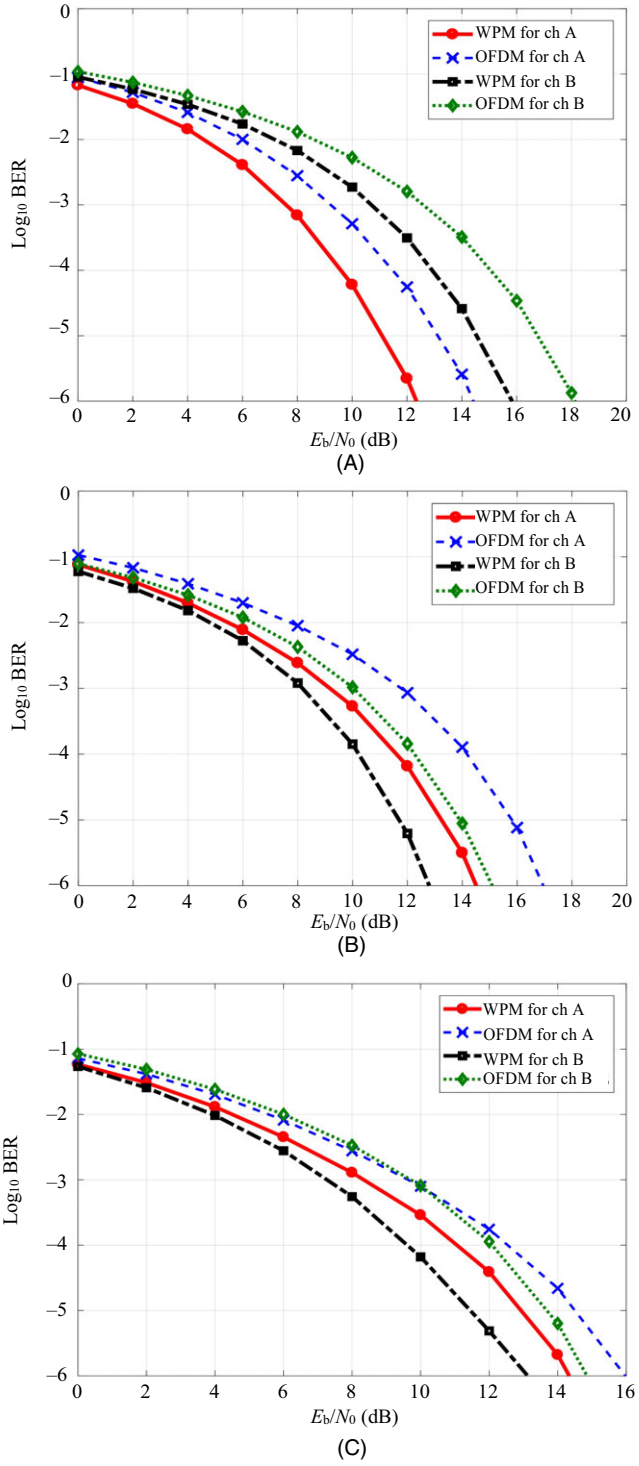

FIGURE 15 BER vs E_b/N_0 comparison between WPM and OFDM for channel A and channel B of (A) indoor office test environment, (B) outdoor to indoor pedestrian test environment, and (C) vehicular test environment

6 | PERFORMANCE ANALYSIS

The analytical BER expression for WPM is used to investigate the benefits of equalization-aware bit loading for WPM. BER plots were obtained for channel A and channel B for the indoor office test environment, outdoor to indoor and pedestrian test environments, and the vehicular test environment considering equalization, with and without bit loading, as shown in Figure 14. From the plots, it can be seen that for each of the test environments, the case of channel A has higher BER reductions when compared to the case of channel B as a result of bit loading. At the BER target of 10^{-5}, for equalization with bit loading, channel A of the vehicular test environment has a maximum reduction in the required E_b/N_0 of more than 10 dB, while channel B of the vehicular test environment has the minimum reduction of the required E_b/N_0 of 1 dB. Overall, for both channel A and channel B for all three test environments, the BER is reduced as a result of bit loading, reflecting the benefits of bit loading.

Furthermore, the BERs with bit loading for WPM are compared with those for OFDM. For WPM, MMSE equalization with equalization-aware bit loading is considered, while for OFDM, one-tap equalization with bit loading is considered. The BERs are plotted for channel A and channel B for all three test environments, and are shown in Figure 15. In most of the cases, the required E_b/N_0 for the BER target of 10^{-5} can be reduced by 1 dB–2 dB for WPM when compared to OFDM. Overall, the numerical results indicate that WPM performs better than OFDM when bit loading is employed by each scheme.

7 | CONCLUSIONS

This paper presents a bit-loading algorithm that is to be used with time-domain linear MMSE equalization. By considering noise amplification and signal attenuation due to equalization error, the bit-loading algorithm can overcome the imperfection of MMSE equalization. While equalization error also introduces ICI, numerical results show that ICI levels are negligible compared to noise powers. Hence, ICI is not considered in the bit-loading algorithm. Numerical results for the BER performances show that even with the equalization error, WPM with bit loading still outperforms OFDM. In particular, analytical expressions were derived to compute the BER, and were verified with results obtained from computer simulations. The BER expressions are then used to investigate the BER performances of WPM and OFDM in different test environments as per Rec. ITU-R M.1225. Numerical results show that in all test scenarios, WPM with a moderate equalizer filter length performs better than OFDM. In addition, in most of the cases, WPM can reduce the required E_b/N_0 by 1 dB–2 dB compared with OFDM at the target BER of 10^{-5}.

ACKNOWLEDGMENTS

This work was partly supported by the Bangkok University Teaching Assistance Scholarship.

ORCID

Sarbagya Buddhacharya http://orcid.org/0000-0002-3678-0083

REFERENCES

1. C. V. Bouwel et al., Wavelet packet based multicarrier modulation, *Proc. Symp. Commun. Veh. Technol. (SCVT)*, Leuven, Belgium, Oct 19, 2000, pp. 131–138.
2. M. Gautier and J. Lienard, Efficient wavelet packet modulation for wireless communication, *Proc. Adv. Int. Conf. Telecommun. (AICT), Morne, Mauritius*, May 13–19, 2007, p. 19.
3. A. Habibi, Introduction to wavelets, *Proc. MILCOM*, SanDiego, CA, USA, Nov. 5–8, 1995, pp. 879–885.
4. A. R. Lindsey, *Wavelet packet modulation for orthogonally multiplexed communication*, IEEE Trans. Signal Process. **45** (1997), no. 5, 1336–1339.
5. B. G. Negash and H. Nikookar, *Wavelet-based multicarrier transmission over multipath wireless channels*, Electron. Lett. **36** (2000), no. 21, 1787–1788.
6. B. Torun, M. K. Lakshmanan, and H. Nikookar, On the analysis of peak-to-average power ratio of wavelet packet modulation, *Proc. Eur. Wireless Technol. Conf.*, Rome, Italy, Sept. 28–29, 2009, pp. 1–4.
7. A. Jamin and P. Mahonen, *Wavelet packet modulation for wireless communications*, Wireless Commun. Mobile Comput. J. **5** (2005), no. 2, 123–137.
8. B. Torun, M. K. Lakshmanan, and H. Nikookar, Peak-to-average power ratio reduction of wavelet packet modulation by adaptive phase selection, *Proc. IEEE Int. Symp. Personal Indoor Mobile Radio Commun. (PIMRC)*, Istanbul, Turkey, Sept. 26–30, 2010, pp. 105–110.
9. M. Gautier et al., PAPR analysis in wavelet packet modulation, *Proc. IEEE Int. Symp. Commun., Contr. Signal Process. (ISCCSP)*, St Julians, Malta, Mar. 12–14, 2008, pp. 799–803.
10. S. Gracias and V. U. Reddy, *An equalization algorithm for wavelet packet based modulation schemes*, IEEE Trans. Signal Process. **46** (1998), no. 11, 3082–3087.
11. A. Bajpai, M. K. Lakshmanan, and H. Nikookar, Channel equalization in wavelet packet modulation by minimization of peak distortion, *Proc. IEEE Int. Symp. Personal, Indoor Mobile Radio Commun. (PIMRC)*, Toronto, Canada, Sept. 11–14, 2011, pp. 152–156.
12. Z. Mohammadi et al., Recovery of ISI channels with wavelet packet modulation using linear equalization and channel estimation, *Proc. Int. Symp. On I/V Commun. Mobile Netw. (ISVC)*, Rabat, Morocco, Sept. 30–Oct. 2, 2010, pp. 1–4.
13. U. Khan, S. Baig, and M. J. Mughal, Performance comparison of wavelet packet modulation and OFDM for multipath wireless channel, *Proc. IEEE Int. Conf. Comput., Contr. Commun. (IC4)*, Karachi, Pakistan, Feb. 17–18, 2009, pp. 1–4.
14. M. K. Gupta and S. Tiwari, *Performance evaluation of conventional and wavelet based OFDM system*, Int. J. Electron. Commun. (AEU) **67** (2013), no. 4, 348–354.
15. R. Ren and S. Zhu, Novel adaptive subcarrier power and bit allocation using wavelet packet parallel architecture, *Proc. Int. Conf. Algorithms Archit. Parallel Process. (ISA3PP 2005)*, Melbourne, Australia Oct. 2–3, 2005, pp. 422–428.
16. M. C. Chang, K. T. Lay, and J. T. Chen, Dynamic water-filling for wavelet communications, *Proc. IEEE Veh. Technol. Conf. (VTC)*, Rhodes, Greece, May 6–9, 2001, 1254–1258.
17. M. Chaffi et al., *Adaptive wavelet packet modulation*, IEEE Trans. Commun. **66** (2018), no. 7, 2947–2957.
18. H. Xian et al., *A kind of PAPR reduction method based on pruning WPM and PTS technology*, J. Electron. (China) **30** (2013), no. 30.
19. J. Zakaria and M. F. M. Salleh, *PAPR reduction scheme: wavelet packet-based PTS with embedded side information data scheme*, IET Commun. **11** (2016), no. 1, 127–135.
20. N. T. Le, Spectrum sensing for wavelet packet modulation schemes, Ph.D dissertation, University of Calgary, Canada, 2017.
21. C. S. Burrus, R. A. Gopinath, and H. Guo, *Introduction to wavelets and wavelet transforms*, Prentice-Hall, NJ, USA, 1998.
22. C. R. Johnson, W. A. Sethares, and A. G. Kelvin, *Software receiver design*, Cambridge University Press, UK, 2011.
23. J. G. Proakis and M. Salehi, *Digital communications*, 5th ed., McGraw-Hill, NY, USA, 2008.
24. A. Goldsmith, *Wireless communications*, Cambridge University Press, UK, 2005.
25. K. D. Wong, *Fundamental of wireless communication engineering technologies*, John Wiley and Sons Ltd, NY, USA, 2012.
26. G. D. Forney and G. Ungerboeck, *Modulation and coding for linear gaussian channels*, IEEE Trans. Inform. Theory **44** (1998), no. 6, 2384–2415.
27. ITU-R Rec. M.1225, Guidelines for evaluation of radio transmission technologies for IMT-2000, (1997).
28. A. R. Lindsey, Generalized orthogonally multiplexed communication via wavelet packet bases, Ph.D. dissertation, Ohio University, 1995.

AUTHOR BIOGRAPHIES

Sarbagya Buddhacharya received his Bachelor Degree in electronics & communication engineering from Pokhara Engineering College, which is affiliated with the Pokhara University, Nepal, in 2006. He received his Master degree in telecommunication engineering from the Asian Institute of Technology, Thailand, in 2010. He worked as a Lab Supervisor in the field of telecommunications at the Asian Institute of Technology, Thailand, from 2011 to 2013. He joined Thaicom Public Company Limited, Thailand, as a senior Engineer in 2013. He has been pursuing his Doctor of Engineering in electrical and computer engineering at the Bangkok University, Thailand, since 2015. His research interests include communication theory, multicarrier modulation, and signal processing.

Poompat Saengudomlert received his BSE degree in electrical engineering from Princeton University, NJ, USA, in 1996, and his MS and PhD degrees in electrical engineering and computer science from the Massachusetts Institute of Technology (MIT), MA, USA, in 1998 and 2002, respectively. From 2002 to 2004, he worked as a postdoctoral researcher for the Laboratory for Information and Decision Systems at MIT, MA, USA. From 2005 to 2013, he worked for the Asian Institute of Technology, Pathum Thani, Thailand. Since 2013, he has been with the Bangkok University-Center of Research in Optoelectronics, Communications, and Computational Systems, Pathum Thani, Thailand, where he is now an associate professor. His main research interests are communication theory, optical communications, and software-defined communications.